COMPORTAREA LA SOLICITAREA LA ÎNCOVOIERE A GRINZILOR DIN BETON ARMAT CONSOLIDATE PRIN METODA NSM CU BARE DIN CFRP ŞI GFRP - STUDII TEORETICE ŞI EXPERIMENTALE

FLEXURAL BEHAVIOUR OF RC BEAMS STRENGTHENED WITH NSM CFRP AND GFRP BARS – EXPERIMENTAL AND NUMERICAL STUDY

SLOBODAN RANKOVIĆ[1]*, RADOMIR FOLIĆ[2], MARINA MIJALKOVIĆ[3]

[1]*University of Niš, Faculty of Civil Engineering and Architecture, 18000 Niš, A. Medvedeva 14, Serbia*
[2]*University of Novi Sad, Faculty of Technical Sciences, 21000 Novi Sad, Trg D. Obradovića 6, Serbia*
[3]*University of Niš, Faculty of Civil Engineering and Architecture, Niš, A. Medvedeva 14, Serbia*

The paper presents the results of experimental and numerical investigations of the reinforced concrete (RC) beams strengthened with the near surface mounted (NSM) carbon and glass FRP bars. Three concrete beams were tested for bending during which the deformations of beams, pattern of cracks and the strains in steel, FRP and concrete were recorded until failure under monotonically increased loading. Additional glass (Ø10mm) and carbon (Ø8mm) FRP bars improved the bearing capacity over the control RC beams by increasing it by 73% and 89%, respectively. A nonlinear analysis model based on FEM is proposed to analyse the behaviour of the strengthened beams. The model was developed using ANSIS software package and the recommended constitutive models therein for concrete, steel and FRP reinforcement. The numerical results obtained using the developed model correlated very well with the experimental results and demonstrated not only significantly increased loading capacity and stiffness, but also considerable ductility of the strengthened beams.

Lucrarea prezintă rezultatele cercetărilor experimentale şi ale analizelor efectuate prin calcul ale unor grinzi din beton armat (RC) consolidate în zona din imediata apropiere a feței inferioare (NSM) cu armături sub formă de bare din fibre de carbon sau de sticlă (FRP). Au fost testate trei grinzi la încovoiere monoton crescător până la cedare, înregistrându-se deformațiile grinzii, configurația fisurilor şi deformațiile specifice în armăturile din oțel sau FRP. Prevederea armăturilor suplimentare sub formă de bare tip FRP (Ø10mm) din sticlă şi (Ø8mm) din carbon au condus la o creştere a capacității portante de 73%, respectiv 89% față de grinda neconsolidată. A fost propusă o metodă de analiză neliniară bazată pe un model FEM pentru a caracteriza comportarea grinzilor consolidate. Modelul a fost dezvoltat utilizând programul de calcul ANSIS considerându-se legile constitutive recomandate pentru beton, oțel şi FRP. Rezultatele analizei numerice efectuate utilizând modelul propus sunt foarte bine corelate cu rezultatele experimentale, demonstrând nu numai îmbunătățirea substanțială a capacității portante a grinzilor consolidate dar şi îmbunătățirea ductilității acestora.

Keywords: *FRP reinforcement, NSM method, flexural strengthening, RC beams, testing, non-linear FEM analysis*

1. Introduction

The well known advantages of the Fibre Reinforced Polymer (FRP) materials over steel reinforcement like their corrosion resistance and the high tensile strength to weight ratio have led to the wider adoption of carbon and glass FRP materials for strengthening of RC beams. Although the initial cost of FRP reinforcement is still higher than the cost of the equivalent steel reinforcement, due to other advantages like easy installation and chemical resistance the FRP materials are already allowing for the cost-effective methods of strengthening RC beams. Alongside the use of FRP materials as the externally epoxy-bonded (EB) plates and strips or prestressing rebars, another recent techniques for the repair and strengthening of RC structures is the use of FRP bars and strips as the additional near surface mounted (NSM) reinforcement [1-6].

NSM FRP reinforcement have certain advantages over the externally bonded FRPs such as, for example: the reduced risks of debonding from concrete, lesser exposure to the environmental and physical damage and, in certain cases such as the strengthening of the upper zones with negative bending moments in continuous beams, are even easier and more practical to install [7-9]. The method of strengthening RC beams with NSM FRP bars or strips involves formation of suitably narrow grooves within the concrete cover which are, after the FRP reinforcement is placed, filled with the epoxy resin or cement paste to provide the bond between reinforcement and concrete [10-13].

There are already several design recommendations on the use of NSM FRP reinforcement [14-15] including the code of practice (ACI, 2008). While most of the earlier studies on the NSM FRP strengthening methods are experimentally based, less research work was published on the numerical modelling and analysis of RC beams reinforced with NSM FRP reinforcement [16-17].

* Autor corespondent/Corresponding author,
Tel. . +381631048215, e-mail: slobodan.rankovic@gaf.ni.ac.rs

This paper deals with concrete beams strengthened by additional FRP reinforcement mounted inside the concrete cover (NSM reinforcement). The study was focused on the beams exposed mainly to flexure. This was done by subjecting specimens to four-point bending test. Tested specimens were chosen and instrument – equipped so that they enable the assessment of the impact of varied parameters on the behaviour of strengthened RC beams. The load-testing of the beams provided the experimental results for comparative assessment of the structural performance for the FRP-strengthened RC beams and the control specimen (concrete beam with steel reinforcement only). The behaviour of strengthened RC beams as a function of fibre type in the applied reinforcing FRP bars was also investigated. Due to the significantly lower cost of GFRP-based bars compared to CFRP-based bars, the behaviour of strengthened beams with additional FRP reinforcement with both carbon (CFRP) and glass fibres (GFRP) was also investigated. This is important for optimal choice of reinforcement in terms of cost. Results of the load tests demonstrate improved structural characteristics of beams with regard to the beam stiffness, ductility and the overall loading capacity.

Finite element method (FEM) models were developed to simulate the behaviour of strengthened beams in linear and nonlinear response until failure under load using the ANSYS software programme [18]. Modelling simplifications and assumptions introduced during this research are presented in later sections. The model of FE method was verified by using experimental research results, which have been presented and analyzed in this paper. Comparisons have been made for deflection in mid-span, strain in FRP reinforcement, appearance and cracks pattern, at different steps of loading for all the values from zero to failure.

2. Experimental Programme

2.1. Material properties

The RC beams were made of concrete with the 28-day cube strength of 30 MPa and the steel reinforcement had the yielding strength of f_{yk} = 400 MPa. The commercially available glass and carbon FRP bars used as NSM reinforcement were Maperod GØ10 and Maperod CØ8 while the Mapewrap11 epoxy and Mapewrap Primer 1 were used as the bonding mortar with the tensile strength of 3 Mpa [19]. the mechanical properties of all materials were experimentally determined before the tests and are listed in Table 1.

2.2. Experimental setup and procedure

The specimens consisted of reinforced concrete beams of total length of 2.950 mm and of rectangular cross-section of 150 × 250 mm. The span between the supports was 2700 mm. The load was applied with two concentrated forces in one third of the span (four-point bending load), through a steel rail, and transferred to the concrete beam through 150 × 100 × 10 mm steel contact plates. The groove is cut in particular direction into concrete cover. The groove is then filled with epoxy paste, the FRP bar is placed in the groove and pressed lightly. This forced the filling material to flow around the FRP bars. After filling the groove the surface was levelled [11]. The groove dimensions were equal to the twofold diameter FRP bars (w/t = 20/20 mm for GFRP and w/t = 16/16 mm for CFRP). The geometry and details of reinforcement beams are shown in Figure 1.

The following beams were tested: 1) B-con beam without added reinforcement, 2) B-G1 beam strengthened within the concrete cover with a glass bar (NSM GFRP) Ø10 mm and 3) B-C1 beam strengthened within the concrete cover with a carbon bar (NSM CFRP) Ø8 mm. The layout of the tested beams under the loading is shown in Figure 2. The loading was in the so-called "time control mode" with a constant growth of deflection at a rate of 0.02 mm/s up to failure.

2.2.1. Test instrumentation

The specimens were tested on a test machine of the range up to 1000 kN, with hydraulic jack application of loading; the range of the measuring cell was up to 100 kN. Deflection was measured with LVDT (linear variable displacement transducers), the strains in concrete, steel and FRP reinforcement were recorded through strain gauges with a length of 100 mm and 6 mm respectively, while data were acquired through the

Table 1

Mechanical properties of concrete, steel and FRP bars.
Caracteristicile mecanice ale betonului, oțelului și barelor din FRP

Material	Diameter *Diametru*	Elastic modulus *Modulul elastic* [GPa]	Tensile failure strain *Efectul de tracțiune la rupere*, $\varepsilon \times 10^{-6}$	Material strength *Rezistența materialului* [MPa]	Manufacturer's data *Datele producătorului*	
					E [GPa]	f_u [MPa]
Carbon FRP bars	Ø8	148.1	13434	1940	150.0	2000
Glass FRP bars	Ø10	47.0	15635	735	40.8	760
Concrete	/	32.8	1220	31.6		
Steel bars	Ø12	205.0	17200	400 (500)		

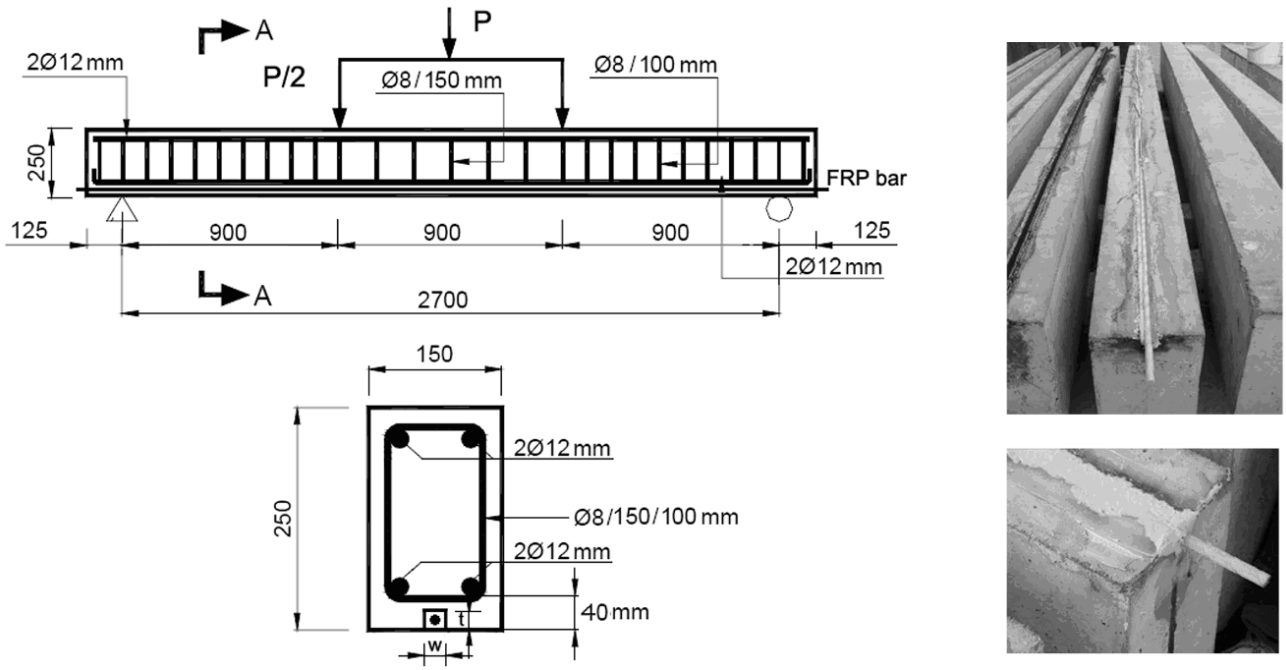

Fig. 1 - Beam details and test setup /*Detalii de armare a grinzii şi de testare*.

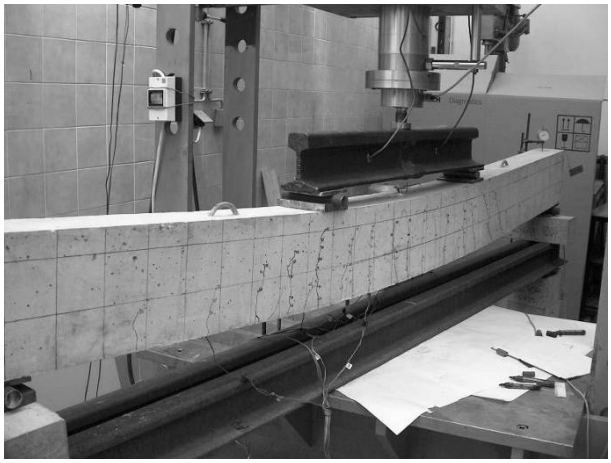

Fig. 2 - Layout of the tested RC beams / *Schema încărcării grinzii din beton armat.*

HBM MGCplus data acquisition system, with an automatic data reading period of one second. Signals were analyzed with HBM CATMAN software.

2.2.2. Experimental setup

During the loading the following was registered: deflections, strains in concrete, strains in steel reinforcement and FRP reinforcement, crack appearance and development – all these as a function of the applied load. In order to register the crack's pattern in concrete, the sides of tested beams were hatched with a square grid at 10 cm from their bottom edge. The sum of width of the cracks along the base of the instrument (100 mm) was registered continuously through a LVDT gauges. The layout of measuring points applied on the beam strengthened with NSM and using FRP reinforcement is shown in Figure 3.

2.3. Test results and their analysis

The results of the measured mid-span deflection, strain in the additional FRP reinforcement, in concrete and in main steel reinforcement, as well as the width of cracks as a function of intensity of load on beams have been analyzed. As noted earlier, types of FRP reinforcement (CFRP and GFRP) have been varied.

Transition between the various stages of loading depends on the strength of concrete, the amount of steel reinforcement, the amount of additional FRP reinforcement, as well as the way it is connected with the surrounding concrete and adhesive, i.e. the adhesion achieved. For example, higher amounts of tensile bars leads to brittle failure (concrete crushing before the steel reinforcement reaches its yield point), low tensile strength of concrete leads to failure (loss of adhesion) at the junction of adhesive (used for coupling the FRP bars) and concrete, while the small slot width leads to failure at the FRP reinforcement - adhesive junction and so on.

2.3.1. Deflection analysis

For the purpose of comparative analysis, Figure 4 shows the results for mid-span deflection obtained by testing beams that were strengthened with the use of various strengthening materials. The comparison was made with regard to a non-strengthened (control) beam, whereby all beams was identically reinforced with steel reinforcement, as described and shown above in Figure 1.

The graphs show the three stages in the load-deflection histories of the tested beams: 1) up to the appearance of the first flexural cracks, the stiffness is nearly identical regardless of the

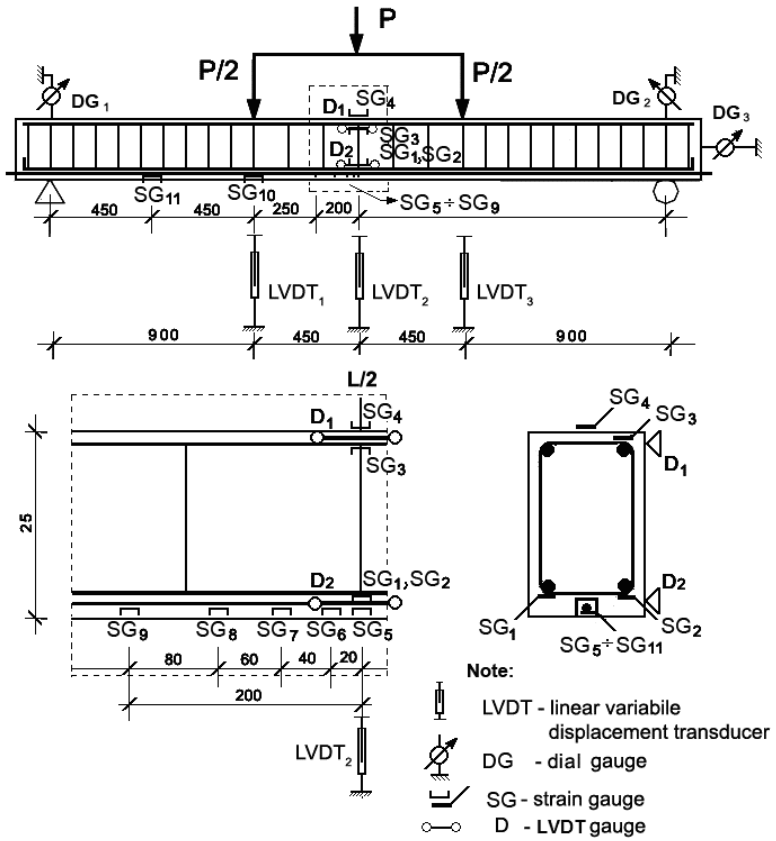

Fig. 3 - Arrangement of instruments for tested strengthened RC beams / *Poziționarea instrumentelor de achiziție date pentru grinda de beton armat consolidată*.

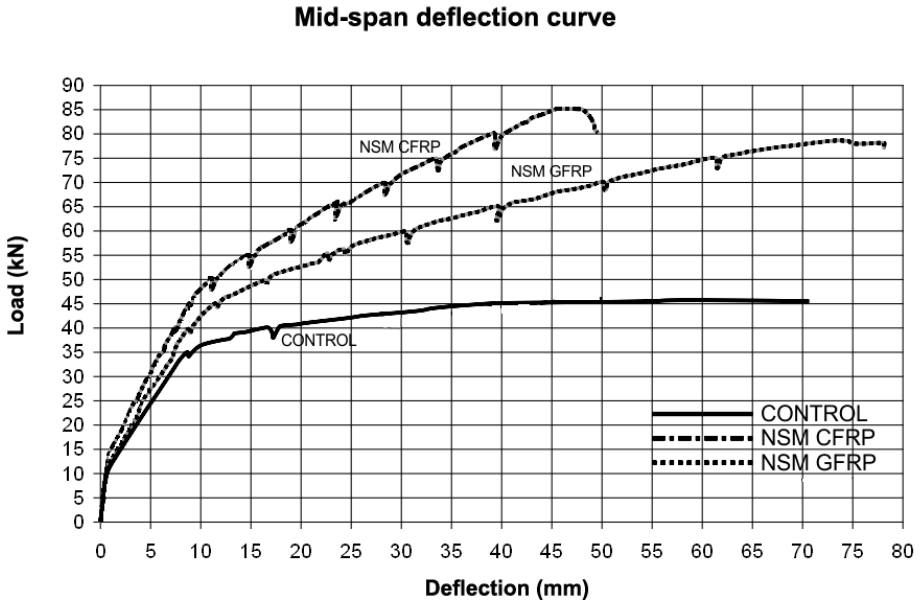

Fig. 4 - Mid-span deflections of the tested steel and FRP reinforced concrete beams / *Deformațiile la mijlocul deschiderii ale grinzilor armate cu bare din oțel şi FRP.*

reinforcement and have perfectly linear behavior; 2) after cracking and until the yielding of the steel rebars the flexural stiffness visibly reduced and provide grater flexural stiffness for strenghtened beams; and 3) the post-yielding stage at which the additional FRP rebars evidently contribute to the increase of the yielding loading and provide much greater flexural stiffness.

The flexural responses of the beams, expressed as the ultimate loading at failure, percentage increase in the loading capacity of FRP-strengthened beams over the reference steel

RC beam, the deflection and the ductility index (ratio of deflections at failure and at the onset of yielding in steel rebars), are graphically compared in Figure 5.

The most remarkable experimental result is the increase of the flexural load capacity after the FRP rebars were added. With the use of a single glass or carbon FRP bar, the ultimate flexural capacity was increased by 73% and 89%, respectively. All values of the ductility index, DI > 4, are found to be appropriate for flexurally loaded RC beams (Jaeger et al., 1995, citated according [20]). As expected, the presence of FRP rebars improved the ductility of beams with the highest value, DI = 6.5, obtained with the glass FRP and DI = 5.3 with carbon FRP. Although the glass FRP bars have much lower modulus of elasticity in comparison to the steel or carbon FRP, they had nevertheless considerably improved the stiffness over the reference steel RC beam. For this reason, the glass FRP bars used as NSM reinforcement, can be a more economical choice for flexural strengthening of RC beams over the carbon FRP because as they provide, at the lower cost, a similar or, at least, comparable strengthening performance.

2.3.2. Analysis of strain in steel reinforcement

From the diagram in Figure 6 it can be seen that strains in steel reinforcement are compatible with those in concrete up to the appearance of cracks, and their values are very low (micro strains of about 80×10^{-6}). With the appearance of first cracks, there is a rapid non-linear growth of strains up to the yielding in steel reinforcement; in the last stage, between reinforcement yield and failure, the nonlinearity is even more prominent. The loss of adhesion between the concrete and reinforcement results in the appearance of cracks and the redistribution of forces from the concrete section to the amount of reinforcement.

2.3.3. Analysis of strain in the FRP reinforcement

The highest number of measuring points was set in order to monitor strains in FRP reinforcement. Strain gauges (SG5 ÷ SG11) were arranged in the zone of maximum bending moment as shown in Figure 3. The values for mid-span and one third-span strains at specific measuring points (SG5) and (SG10) for different FRP materials are compared in Figure 7.

The growth of strain in GFRP bars remains similar to strain in CFRP bars up to the yielding limit of steel reinforcement; after that it exhibits a much more prominent non-linearity and higher maximum value.

One third-span strains in FRP reinforcement at the cross-section beneath the concentrated force are shown in Figure 7-b; these were obtained at strain gauge SG10. Given the same effects of bending moment, and the negligible impact of transverse forces, the qualitative form of the diagram is considerably similar to the previous (mid-span) one. The maximum values of strains in additional FRP reinforcement was 1.2% for CFRP and 2% for GFRP.

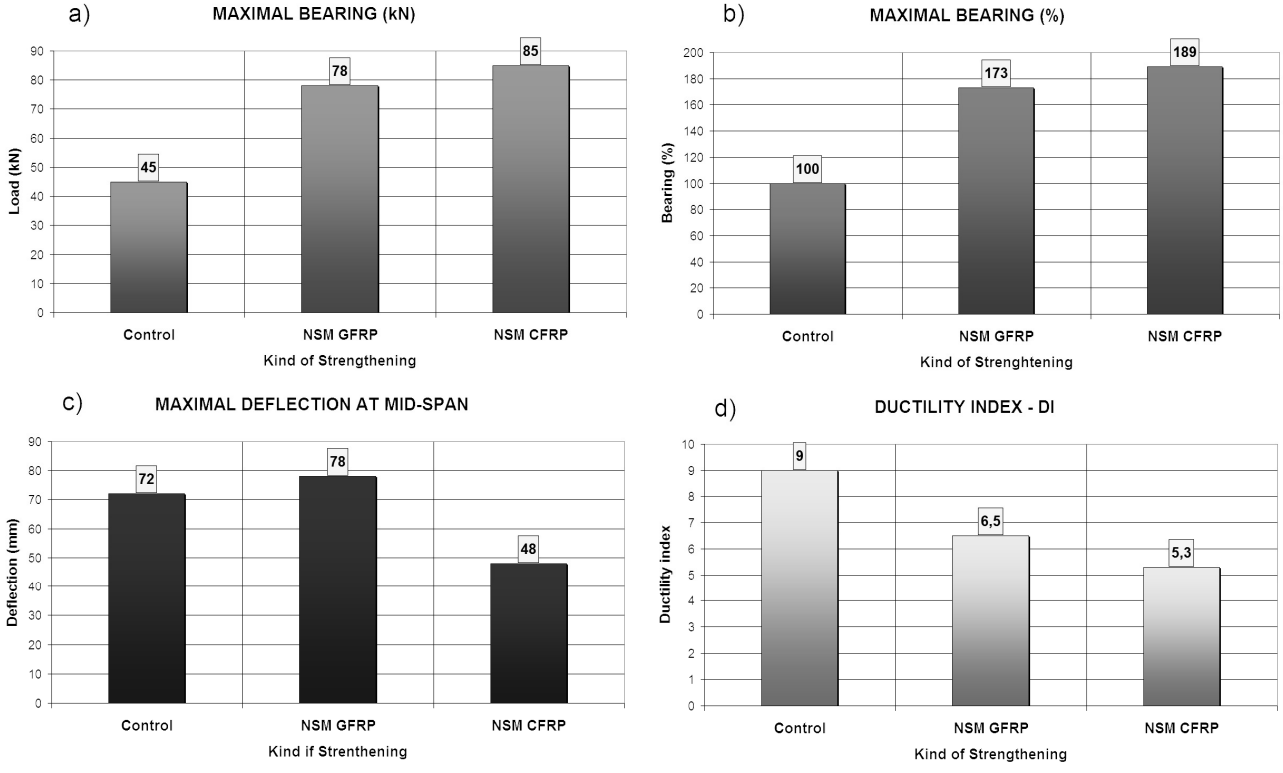

Fig. 5 - Comparing the measured values for bearing capacity, deflection and ductility / *Comparație între valorile măsurate ale capacității portante, deformațiilor şi ductilității.*

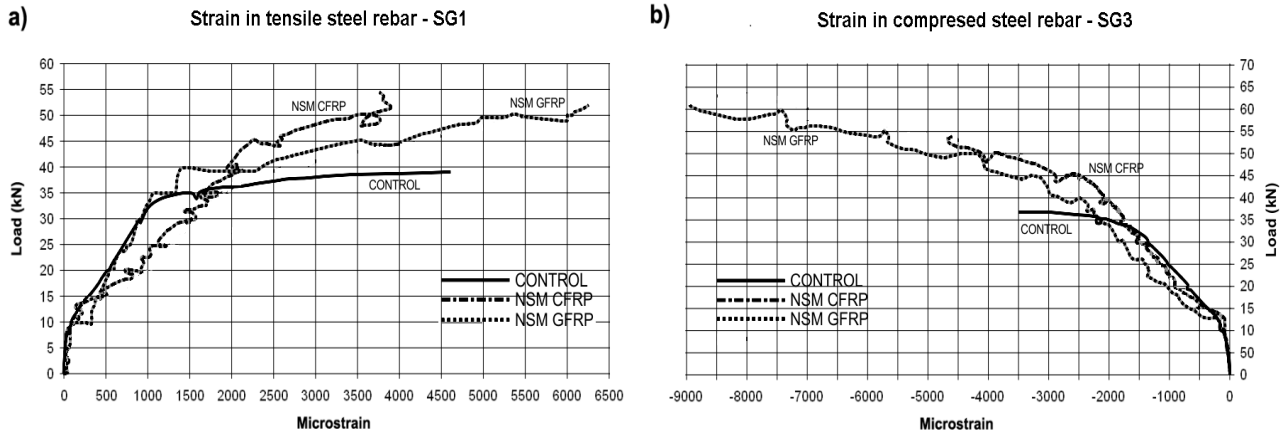

Fig. 6 - Mid-span strain diagram of tensioned (SG1) and compressed (SG3) steel reinforcement / *Deformațiile specifice ale armăturii din oțel întinse şi comprimate în zonele din mijlocul grinzii*.

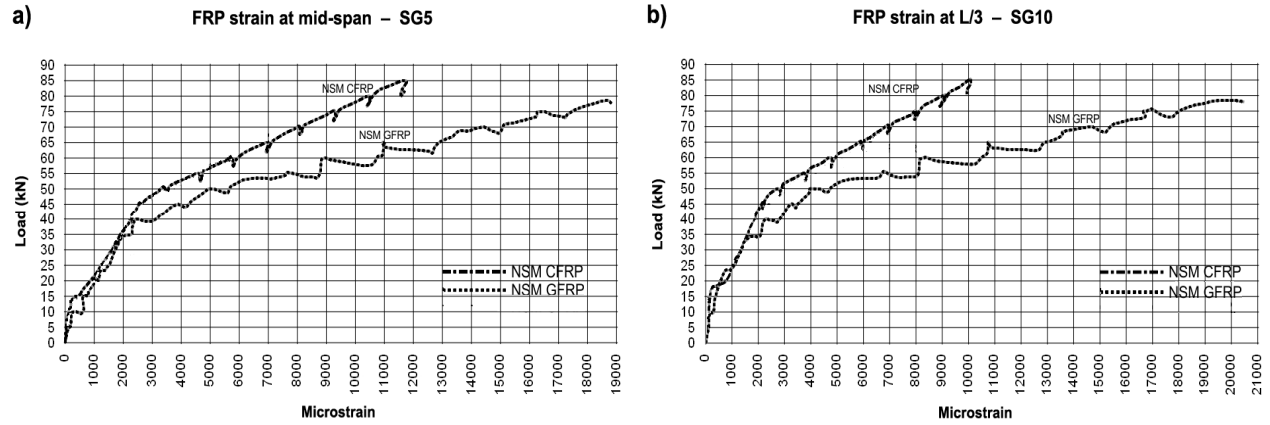

Fig. 7 - Mid-span and one third-span strain diagram for FRP reinforcement / *Deformațiile unitare ale armăturii din FRP la jumătatea şi respectiv la o treime din deschiderea grinzii.*

One sixth-span strains of the FRP reinforcement (i.e. at the distance of 45 cm from the support), are shown side by side in Figure 8 (SG11). From the diagram it is evident that the linear load-strain relationship, i.e. the appearance of the first crack, occurs at a higher level of loading when strengthening was accomplished with CFRP reinforcement than when the strengthening was done with GFRP reinforcement. The zone of non-linear development of strains in the additional CFRP reinforcement occurs when the load exceeds 30 kN, which is twice as much as the strengthening with GFRP reinforcement.

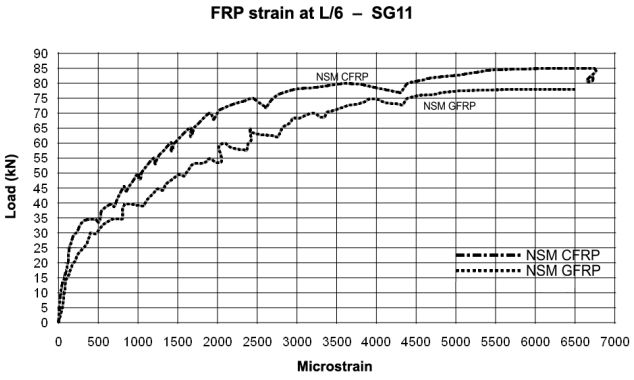

Fig. 8 - One sixth-span strain diagram for FRP reinforcement (SG11 at the distance of 45 cm from the support) / *Diagrama încărcare deformație specifică a armăturii FRP la 1/6 din deschiderea grinzii (SG11 la o distanță de 45 cm de reazem).*

2.3.4. Analysis of strain in concrete

The characteristic strain in the compressed area of concrete is presented for the mid-span measuring point at the upper surface of the concrete beam SG4, and it was measured at the top concrete fibre at midspan (Figure 9a). In addition, pressure strains in concrete were also measured at the distance of 20 mm from the upper beam-edge (D1) (Figure 9b). Qualitatively, the shape of the concrete strain diagram is similar to the reinforcement strain diagram. Before the appearance of the first crack, the load-strain relationships are almost linear; the second part of the diagram starts with the first crack and ends at the yield limit in steel reinforcement when strain increases noticeably (Figure. 9); the third rapid growth of strains occurs at the reinforcement yield limit up to beam failure. In the presence of FRP

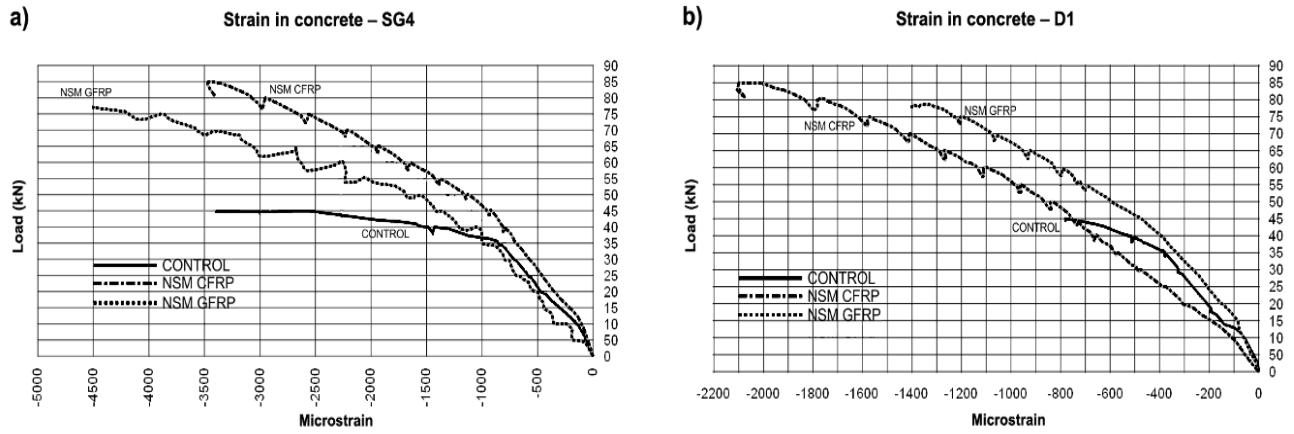

Fig. 9 - Strains in compressed concrete – measuring points SG4 and D1 / *Deformații specifice în betonul comprimat-măsurate în punctele SG4 şi D1.*

rebars, the maximum compression strains in concrete were increasing at slower rates than was the case for reference RC beam with internal steel rebars only e.g. the greater applied load was required after FRP-strengthenig to achieve the same level of compression strains in concrete at the mid-span section.

2.3.5. The analysis of the crack patterns in the mid-span of the concrete

The FRP rebars have also reduced the widths of flexural cracks which were measured visually with the micrometer magnifier. In the mid-span zone, the crack widths were also electronically sampled with a 100 mm-base LVDT (D2) glued onto the concrete surface. This approach is possible because the elongation in concrete was negligible before the appearance of the first cracks and the crack spacing was larger than the instrument's base length. The measured crack widths in NSM CFRP and GFRP strengthened beams and their comparison with the crack widths from the control (non-strengthened) beam are shown in Figure 10.

As indicated by the "loading – crack width" diagram, when applying the NSM method with GFRP additional reinforcement, the results were poorer in terms of serviceability, but the improvement is still significant as compared to the control beam. Strains measured in this way (on the concrete surface) are very similar to strains in FRP reinforcement due to the negligible values of tensile strain received by the concrete, as noted earlier. Before cracking, the strains in the reinforcement are compatible with the strains in the surrounding concrete, and are therefore of negligible magnitude.

As indicated by the diagram in Fig. 10, yielding in CFRP and control beams occurs when cracks of 0.3 mm appear, while in case GFRP this value is about 0.5 mm.

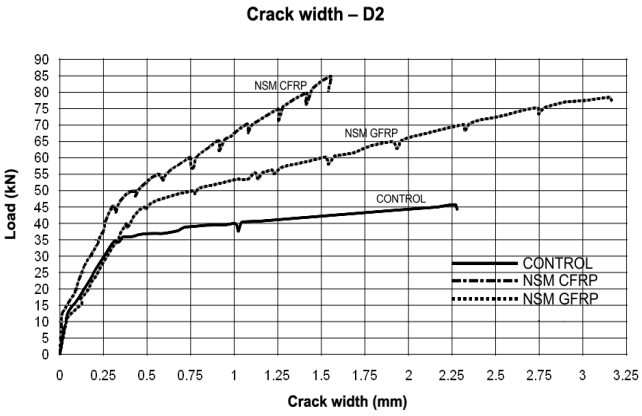

Fig. 10 - Loading-crack width diagrams / *Diagrama încărcare-deschidere fisuri.*

2.4. The modes of failure and load capacity

- **B-G1:** Beam strengthened with Ø10 mm GFRP reinforcement

The beam deflection under loading is shown in Figure 11, while the typical crack distribution is shown in Figure 12. The beam strengthened with GFRP reinforcement and the failure mechanism that occurs under the test load is shown in Figures 13 and 14, respectively. Notably, the beam is highly deformable with very good ductility, the crack distribution is uniform and the failure is caused by the exceeding tensile stress on the concrete-epoxy interface in the groove. Transverse cracks on the bottom of the beam do not intersect with the groove containing the strengthening and the epoxy filling; instead, they run along the concrete-epoxy interface (Fig. 13). These cracks occur after the onset of yielding in steel reinforcement at an angle of approximately 45° and does not intersect epoxy adhesive has a

Fig. 11 - Beam deformation under loading / *Deformația grinzii sub încărcări* (Δ_{max}= 78 mm).

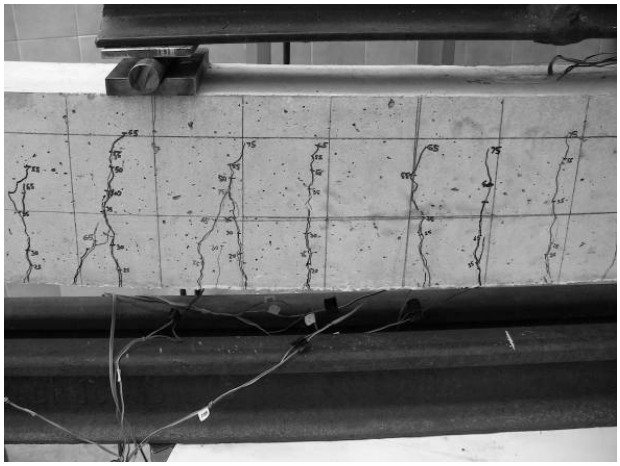

Fig. 12 - Typical crack pattern (δ_{max}=3.2 mm)/*Configurația specifică a fisurilor.*

Fig. 13 - Beam failure resulting from the loss of concrete-epoxy joint / *Cedarea grinzii datorată pierderii conlucrării între beton şi epoxi.*

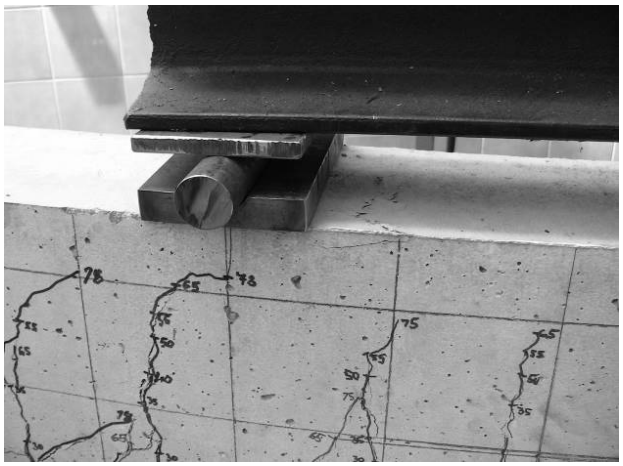

Fig. 14 - Concrete crumbling in the area of application of force (near the supporting slab) / *Zdrobirea betonului în zona de aplicare a forței (lângă reazem).*

higher tensile strength compared to concrete. Due to the surface roughness of the GFRP reinforcement, the loss of adhesion at the epoxy bond failed to occur. At higher loads, a concrete crushing occurs at force application points around the supporting slab (F14).

- **B-C1:** Beam strengthened with Ø8 mm CFRP reinforcement

The failure mechanisms in the RC beam in the case of using a smooth CFRP reinforcement is shown in Figures 15 to 18. The failure occurs due to a sudden slip at the CFRP reinforcement-epoxy interface in the anchoring zone at the beam's end (Fig. 16), while in the zone of pure bending the failure is due to separation at the epoxy-concrete interface of (Fig. 17). This leads to the parallel splitting/spalling of the concrete cover. The beam's bearing capacity is very high (P_{max} = 85 kN), but the failure is sudden, accompanied by strong burst and an extensive damage to the beam. Prior to the failure, the beam ductility is acceptable (DI = 5.3).

- **B-con:** Control beam (benchmark)

The typical shape of the cracks and their appearance from the bottom (tensioned) side of the beam in the zone of pure bending are shown in Figures 19 and 20. The maximum force applied was 45 kN, after which deformations developed without increasing the load. Cracks are evenly distributed transversely across the width of the beam, and the failure is ductile, i.e. DI = 9.

3. Numerical Investigations

3.1. Introduction

For the numerical analysis of tested RC and FRP-strengthened beams, a non-linear FE analysis was carried out with ANSYS [18]. This software package supports the 'smeared-crack' concrete model for tension and has been used in several studies [21-22] of RC beams strengthened with the internal or externally bonded FRP composites. In the 3D models of tested beams, the

Fig. 15 - Failure resulting from the loss of adhesion of CFRP reinforcement (before slipping crack width is δ_{max}=1.1 mm) / *Cedarea datorată pierderii aderenței armăturii din CFRP (Înainte de alunecare deschiderea fisurilor a fost δ_{max}=1.1 mm).*

Fig. 16 - Slipping of the CFRP reinforcement due to the loss of bond at the joint with the epoxy resin / *Alunecarea armăturii din CFRP datorită pierderii conlucrării cu raşina epoxi.*

Fig. 17- Separation of concrete at the height of the concrete cover and crack distribution (front side of the beam) / *Separarea betonului pe înățimea stratului de acoperire cu beton a armăturii şi distribuția fisurilor (pe partea din față a grinzii).*

Fig. 18 - Separation of concrete at the height of the concrete cover (back side of the beam) / *Separarea betonului pe înălțimea stratului de acoperire cu beton a armăturii şi distribuția fisurilor (pe partea din spate a grinzii).*

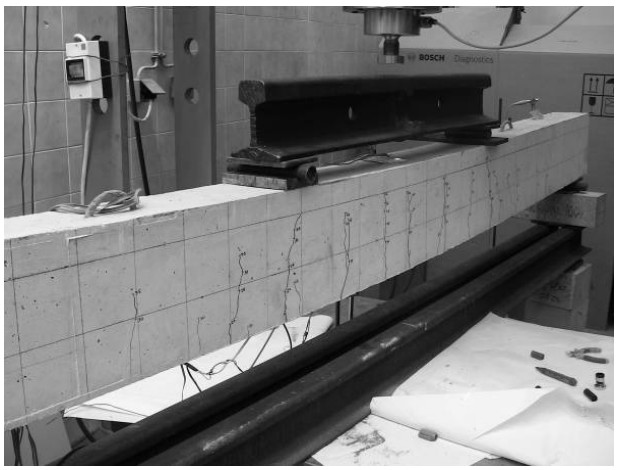

Fig. 19 - Crack distribution on the control beam (δ_{max}=1.8 mm) / *Distribuția fisurilor pe grinda de control.*

Fig. 20 - Typical cracks in the zone of pure bending on the tensioned (lower) side of the control beam after the bearing capacity is exhausted / *Distribuția fisurilor pe fața inferioară a grinzii în momentul atingerii capacității portantă a grinzii.*

steel and epoxy adhesive are modelled as the elasto-plastic materials, FRP rebars as ideally elastic and the concrete models for compression and tension, proposed in [23] were used. The exact geometry of the epoxy adhesive layer, situated in the longitudinal groove between the FRP bars and the surrounding concrete layer, was modelled with the 3D solid elements. A perfect bond between the steel/FRP rebars (modelled as truss links) and concrete is assummed counting that the differential slip between them will be achieved by the tensile yielding properties of the adhesive and the concrete tension stiffening model.

3.2. Material models

3.2.1. Concrete

The concrete stress-strain constitutive relations and failure criteria were defined by the simplified compression and tension law [21], (Fig. 21). The following mechanical properties of concrete were used in the analysis: Maximum compressive strength of concrete: f_c = 36.1 MPa; Tensile strength of concrete: f_t = 3.51 GPa; Elastic modulus of concrete: E_c = 32.8 GPa; Poisson's ratio: v_c = 0.2.

A simplified shear retention law (reduction of shear stresses across the crack plane) was defined in ANSYS with the following parameterrs: βc = 0.95, βt = 0.2, Tc = 0.6 [22].

For solid modelling of concrete as a quasi-brittle material (with different stress-strain law s for compression and tension), the SOLID65 8-noded 3D element was used. The internal tensile steel reinforcement in concrete is modelled with the 2-noded "LINK8" 3D truss elements which are embedded into concrete.

3.2.2. Steel reinforcement and steel plates

For steel reinforcement and support plates, steel grade S235 was adopted with the modulus of elasticity Es = 210 GPa, Poisson's ratio v = 0.3 and the yielding and ultimate tensile strengths of f_y = 235 MPa and f_{yk} = 400 MPa.

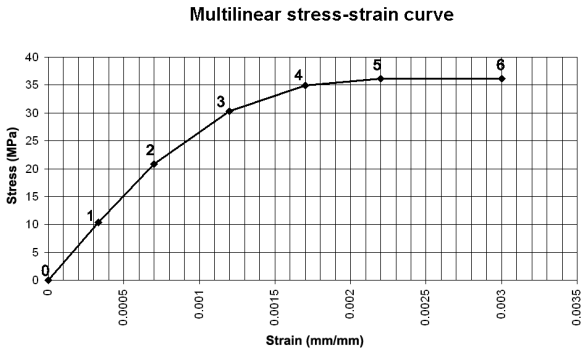

Fig. 21 - The stress-strain multilinear curve for concrete / *Diagrama efort unitar deformație specifică a betonului.*

3.2.3. Composite FRP reinforcement

The FRP materials are modelled as ideally elastic orthotropic materials using 8-noded SOLID45 elements. The modulus of elasticity in the direction perpendicular to the fibres was taken as 77% for CFRP and 33% for GFRP bars, of the modulus in the principal fibre direction [21].

3.3. Mesh geometry, loading and boundary conditions

Several mesh densities were tried in the analysis and, exploiting the double symmetry, only one quarter of each RC beam was modelled with the full bond assumed between the materials. A non-linear analysis followed the methodology of other authors [21], [22] with 1,966 elements and 2,361 nodes was adopted (Fig. 22), and the load was applied incrementally in steps of 100 N to maintain convergence.

3.4. The FE analysis results

The accuracy of the non-linear FE analysis is assessed by comparing calculated beam deflections and strain in the FRP reinforcement with the experimentally measured values. As expected, until the appearance of the first flexural

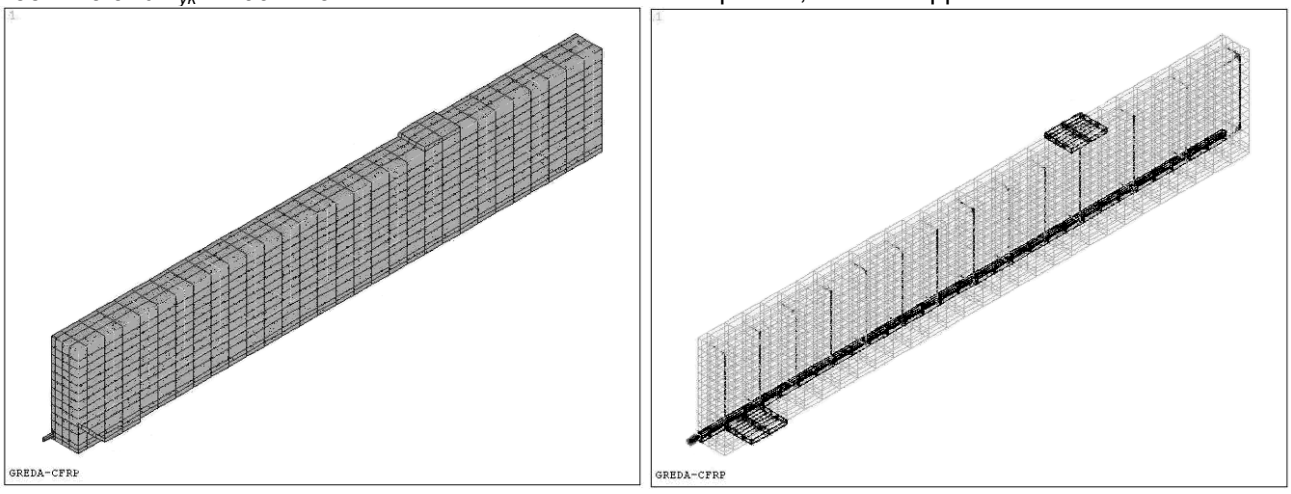

Fig. 22 - Model for the finite element analysis of quarter RC beam / *Model pentru analiza de tip element finit a unui sfert din grinda din beton armat.*

cracks, the structural response was linear and the numerical results are in full agreement with the measurements. Close correlation between the computed and measured deflection values for both beams were obtained until the yielding of the main steel reinforcement. Only after yielding of steel reinforcement, the stiffness of the FE analysis model is somewhat larger but, during this stage, the effects of strengthening with FRP reinforcement on increasing the beam stiffness and loading capacity were most obvious.

3.5. Comparative results of the experimental and numerical analysis

3.5.1. Deflection

The comparison of the numerical and experimentally measured deflections for beam B-C1 (strengthened with the NSM carbon FRP bars).

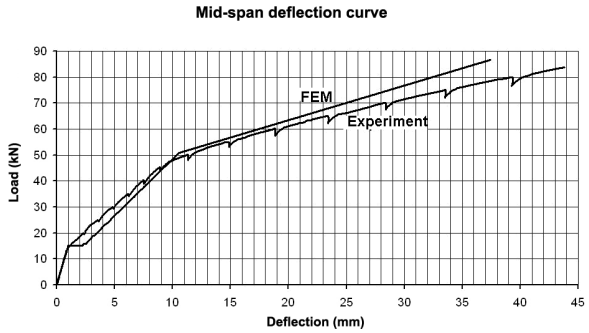

Fig. 23 - Comparative diagrams of the mid-span deflection obtained experimentally and by the FEM analysis / *Comparație între diagramele încărcare deformație la jumătatea deschiderii obținute experimental şi prin analiza FEM.*

It can be seen from the deflection plots in Figure 23 that the FE analysis has accuractely estimated the load corresponding to the first flexural cracks (15 kN) and to the yielding of steel reinforcement (50 kN). The conclusion about the post-yielding beam response is that FRP rebars have significantly increased the stiffness of the beam but the assumption of full bend between the steel or FRP reinforcement and concrete led to the somewhat higher overall stiffness of the beam.

3.5.2. Strains

The plots of measured and calculated strains in the carbon FRP reinforcement show the similar trend as the deflection (Fig. 25). After the yielding of steel reinforcement, the FE analysis model shows the higher stiffness due to the full bond between the reinforcement and concrete. Still, this trend is conservative with regard to the calculated tensile strains and stresses in the epoxy bonding resin (Figure 26) which, with the full bond assumption, picked up higher tension from the FRP reinforcement. The maximum tensile strains (stresses) in the epoxy layer are less than the limiting value meaning that the full bond with the FRP rebar is maintained.

3.5.3. Cracks

The pattern formation of flexural and shear cracks is graphically presented for some characteristic loading values and the numerically obtained crack patterns closely match the experimental observations (Fig. 27). Vertically aligned cracks first appear in the area of the maximum bending moment and, during the later

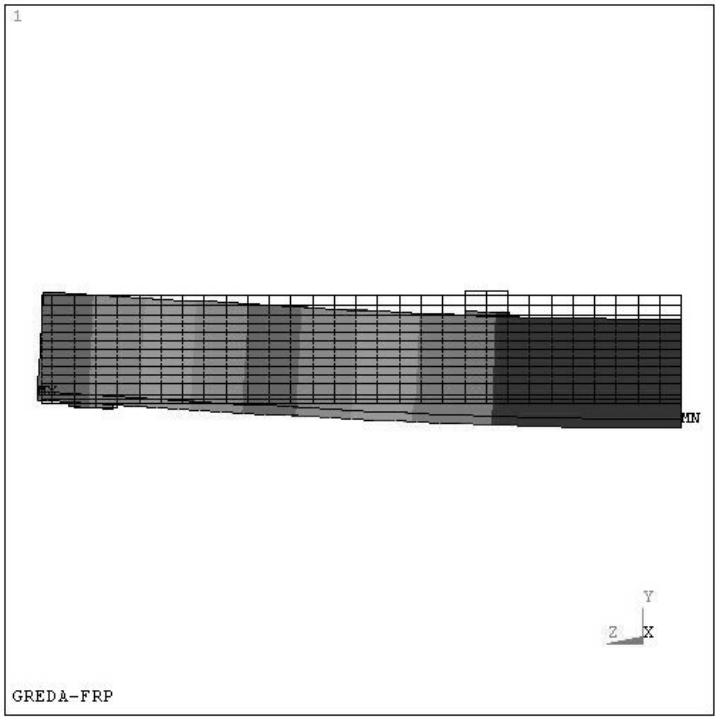

Fig. 24 - Beam deflection obtained through the analysis of the FEM model [cm] / *Deformația grinzii obținute prin analiza modelul.*

loading stages, they spread towards the beam supports as the diagonal shear cracks (Fig. 28). The first crack is shown by a red circle, the second by a green circle, and the third by a blue circle [18]. The lengths of the ctacks are similar to those observed experimentally.

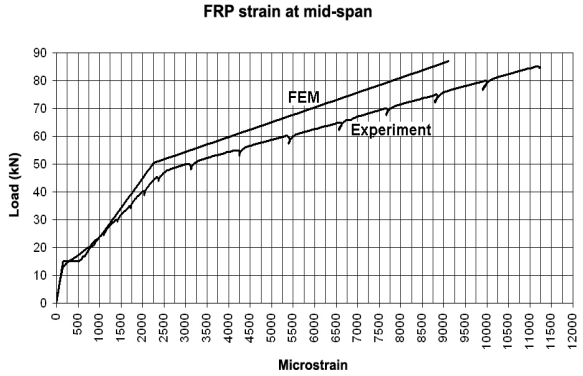

Fig. 25 - Comparative mid-span strain diagrams for the CFRP reinforcement obtained experimentally and numerically (by FEM analysis) / *Comparație între diagramele deformațiilor specifice pentru armătura de tip CFRP la jumatatea deschiderii obținute experimental şi prin analiza FEM.*

4. Conclusions

By means of experimental testing and numerical analysis, this work investigated the effectiveness of the glass and carbon FRP rebars for strengthening RC beams. It was demonstrated that the NSM FRP reinforcement can significantly increase the loading capacity and stiffness of the RC beams while also improving their behaviour in terms of serviceability and ductility at the ultimate limit state.

The non-linear FE analysis was conducted to assess the development of tensile stresses in the anchorage zone of the FRP rebars which lead to the tensile failure of the concrete cover layer or the loss of bond between the FRP rebar and concrete. The following conclusions were made for reinforced concrete beams featuring internal steel and additional FRP rebars:

1. The application of FRP materials as NSM reinforcement is practical strengthening technique that can, even with small amounts of additional reinforcement, substantially increase the

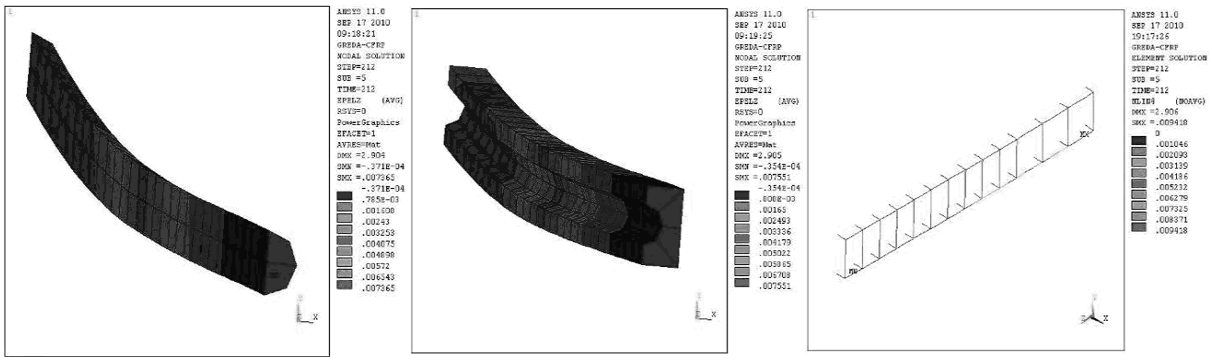

Fig. 26 - Strains in the CFRP reinforcement, epoxy raisin and steel reinforcement obtained by FEM analysis / *Deformații specifice ale răşinii, armăturii din oțel şi CFRP obținute prin analiza FEM.*

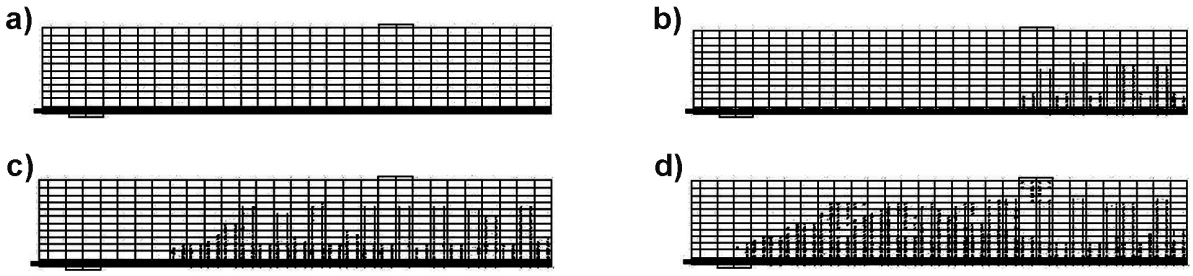

Fig. 27 - Crack pattern as the function of loading: a) P = 15 kN, b) P = 40kN c) P = 60kN, d) P = 85kN / *Distribuția armăturilor în funcție de nivelul încărcării: a) P = 15 kN, b) P = 40kN c) P = 60kN, d) P = 85kN.*

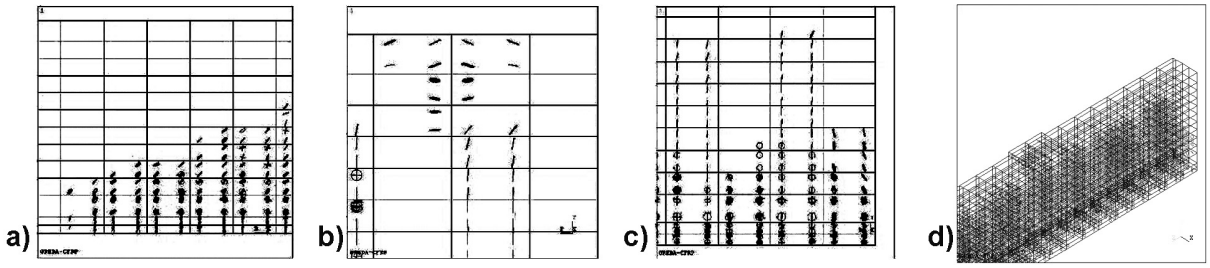

Fig. 28 - Typical cracks: a) shearing; b) compressive; c) bending; d) axonometric / *Fisuri tipice: a) de forfecare; b) de compresiune; c) de încovoiere; d) axonometric.*

over flexural capacity of the existing RC beams. This is confirmed by our results from the use of Ø10 mm glass and Ø8 mm carbon FRP rebars that achieved increases of the loading capacities between 73% and 89% over the reference steel RC beam.

2. While either glass or carbon FRP can be used as NSM reinforcement to achieve a certain ultimate loading capacity of the strengthened RC beam, the choice of the material can be influenced by other requirements. Due to the lower price, the glass FRP can be the more economical material for most strengthening situations but whenever the deformability and deflection of the beam need to be limited, carbon FRP rebars are advantageous because of their much higher modulus of elasticity.

3. Strengthening with additional NSM glass or carbon FRP rebars does not have unfavourable effects on the ductility of RC beams. The ductile behaviour of strengthened RC beams, or the loading capacity after the yielding of internal steel reinforcement, was experimentally observed with both types of NSM FRP rebars. As expected because of their lower modulus of elasticity, higher values of the ductility index (DI) were measured when glass FRP rebars were used as NSM reinforcement in comparison with carbon FRP repars (DI = 6.5 for glass versus, DI = 5.3 for carbon FRP).

4. While the use of NSM FRP reinforcement can lead to brittle failure modes for the strengthened RC beams, the exhibited failure modes were somewhat different for the two types of FRP rebars. When the glass FRP rebars was used as NSM reinforcement, the failure occurred in the anchorage zone due to the loss of bond at the concrete-epoxy resin interface. For the RC beam strengthened with carbon FRP rebars, the failure was due to the loss bond between the carbon FRP rebar and the surrounding epoxy resin. In the case of carbon FRP NSM reinforcement, the loss of bond can be explained by very low adhesion between the smooth surface of carbon FRP rebars and the epoxy mortar.

5. The brittle failures of NSM glass and carbon FRP reinforcement in the anchorage zone are undesired failure modes because they take place before the full flexural capacity of the strengthened RC beams is utilised. Therefore, it is recommended that the model for non-linear FE analysis is used in the strengthening study and/or design of RC beams with additional NSM FRP reinforcement to address the brittle failure modes in the anchorage zone of FRP rebar. By demonstrating good accuracy between the calculated and measured load-deflection curved for RC beams with both internal steel and NSM FRP rebars, it was shown that the NL FE analysis can be a reliable tool for assessing the development of tensile and shear stresses in concrete and epoxy layers that lead to brittle failures in the anchorage zone.

Acknowledgements

We would like to express our appreciation and thanks to the MAPEI Company that provided the FRP material and epoxy for the research presented in this paper.

The research presented in this paper is a part of the investigation within the research project TR 36043 supported by the Ministry for Science and Education, Republic of Serbia. This support is gratefully acknowledged.

REFERENCES

1. ACI 440.1R-06. Guide for the Design and Construction of Structural Concrete Reinforced with FRP Bars, ACI Committee 440, American Concrete Institute, Farmington Hills, MI; 2006. p. 44.
2. ACI 440.2R-08. Guide for the Design and Construction of Externally Bonded FRP Systems for Strengthening Concrete Structures, ACI Committee 440, American Concrete Institute, Farmington Hills, MI; 2008. p. 45.
3. Fib, Bulletin n.14 (Task Group 9.3). Externally bonded FRP reinforcement for RC structures. Technical report on the design and use of externally bonded fibre reinforced polymer reinforcement (FRP EBR) for reinforced concrete structures. International Federation for Structural Concrete, Lausanne; 2001.
4. ISIS Educational Module 4. An Introduction to FRP Strengthening of Concrete Structures. A Canadian Network of Centres of Excellence; 2004.
5. A. Nanni, North American Design Guidelines for Concrete Reinforcement and Strengthening Using FRP: Principles, Applications, and Unsolved Issues. Journal of Construction and Building Materials 2003, **17**(6-7), 439.
6. G. Oprişan, N. Ţăranu, M. Budescu, and I. Entuc, Structural behavior of reinforced concrete beams strengthened by CFRP plate bonding, Romanian Journal of Materials 2012, **42**(4), 387-398
7. H. Nordin, B. Täljsten, and A. Carolin, Concrete beams strengthened with prestressed near surface mounted reinforcement (NSMR). International Conference on FRP Composites in Civil Engineering J.-G. Teng (Ed), 2001, (2), 1067.
8. A. Carolin, H. Nordin, and B. Täljsten, Concrete beams strengthened with near surface mounted reinforcement of CFRP. International Conference on FRP Composites in Civil Engineering , J.-G. Teng (Ed), 2001, **2**, (5-4), 1059.
9. S. Ranković, R. Folić, and M. Mijalković, Efects of RC beams strengthening using near surface reinforced FRP composites, FACTA UNIVERSITATIS 2010; **8**(2), 177.
10. R. El-Hacha, and S.H. Rizkalla, Near-Surface-Mounted Fiber-Reinforced Polymer Reinforcements for Flexural Strengthening of Concrete Structures. ACI Structural Journal 2004, **101**(5), 717.
11. L. De Lorenzis, and J.G. Teng, Near-surface mounted FRP reinforcement: an emerging technique for structural strengthening. Composites: Part B: Engineering 2007, **38**, 119.
12. D. Glavardanov, and R. Folić, Strengthening concrete structures with FRP element and NSM technique. Materijali i konstrukcije 2007, **4,** 29.
13. J.A.O. Barros, Fortes AS. Flexural strengthening of concrete beams with CFRP laminates bonded into slits. Cem Concr Compos 2005, **27**(4), 417.
14. R. Parretti, and A. Nanni, Strengthening of RC members using nearsurface mounted FRP composites: design overview. Adv Struct Eng 2004, **7**(6), 469.
15. F. Al-Mahmoud, and A. Castel, R. François, and C. Tourneur, Strengthening of RC members with near-surface mounted CFRP rods. Composite Structures 2009.

16. B. Taljsten, A. Carolin, and H. Nordin, Concrete structures strengthened with near surface mounted reinforcement of CFRP. Adv Struct Eng 2003, **6**(3), 201.
17. A. Si-Larbi, A. Agbossou, E. Ferrier, and L. Michel, Strenghtening RC beams with composite fiber cement plate reinforced by prestressed FRP rods: Experimental and numerical analysis. Composite Structures 2012, **94**, 830.
18. ANSYS, Swanson Analysis System, US, 2003.
19. Mapei FRP System, www.mapei.com
20. S. Ranković, Experimental and theoretical analysis of limit state RC linear plane structures strengthened with NSM FRP elements. Faculty of Civil Eng. and Architecture, Niš, PhD Theses 2011, p. 177.
21. D. Kachlakev, and T. Miller, FE Modelling of Reinfoced Concrete Structures, Strengthened with FRP Laminates. Final Report SPR 316, Oregon State University, Department of Transportation 2001.
23. A. Wolanski, Flexural behaviour of reinforced and prestressed concrete beams using finite element analysis. Master thesis, Marquette University, Milwaukee, Wisconsin 2004.
24. K.J. William, and E.P.Warnke, Constitutive Model for the Triaxial Behavior of Concrete. Proceedings, International Association for Bridge and Structural Engineering, ISMES, Bergamo, Italy, 1975, **19**, 174.

****

MANIFESTĂRI ŞTIINȚIFICE / SCIENTIFIC EVENTS

2014 International Concrete Sustainability Conference, May 12-15, in Boston, USA.

The 9th annual conference will be held in conjunction with the *MIT Concrete Sustainability Hub 2014 Industry Day* scheduled for May 15, 2014. The *International Concrete Sustainability Conference* provides learning and networking opportunities on the latest advances, technical knowledge, continuing research, tools and solutions for sustainable concrete manufacturing, design and construction.

Researchers, academics, students, engineers, architects, contractors, concrete producers, public works officials, material suppliers and concrete industry professionals are invited to attend, submit papers and give presentations.

Topics

Experts will present on the latest developments related to design, specifying, manufacturing, testing, construction, maintenance, and research of concrete as it relates to sustainable development.

LIFE CYCLE ASSESSMENT Assessing carbon footprint, embodied energy and other environmental impacts for buildings, infrastructure, and cement and concrete manufacturing.

LOW IMPACT DEVELOPMENT Pervious pavements and erosion control structures. Urban heat island reduction, light colored pavements, green roofs and cool communities.

GREEN CONCRETE Recycled and alternative materials including aggregates, water, cementitious materials, and fuels. Beneficial use of byproducts for cement and concrete production.

NEW CONCRETE TECHNOLOGY Durability, extended service life models and validation, performance based specifications to foster sustainability. Innovative concrete production methods.

SUSTAINABILITY INITIATIVES Green building codes and standards adopted by building owners, designers, contractors and product manufacturers. Economic incentives and legislation.

FUNCTIONAL RESILIENCE High performance concrete applications in buildings and infrastructure, fortified building codes, and community initiatives focusing on disaster resistance and adaptive reuse.

Contact: http://www.concretesustainabilityconference.org

****